catalysts

MDPI

Article

Pt/C and Pt/SnO_x/C Catalysts for Ethanol Electrooxidation: Rotating Disk Electrode Study

Artem S. Pushkarev [1,2], Irina V. Pushkareva [1,2], Natalia A. Ivanova [2], Stephanus P. du Preez [3], Dmitri Bessarabov [3], Ratibor G. Chumakov [2], Vladimir G. Stankevich [2], Vladimir N. Fateev [2], Anatoly A. Evdokimov [4] and Sergey A. Grigoriev [1,2,*]

1 National Research University "Moscow Power Engineering Institute", 14, Krasnokazarmennaya st., Moscow 111250, Russia; pushkarev_as@outlook.com (A.S.P.); pushkareva_iv@outlook.com (I.V.P.)
2 National Research Center "Kurchatov Institute", 1, Akademika Kurchatova sq., Moscow 123182, Russia; ivanovana.1989@outlook.com (N.A.I.); Chumakov_RG@nrcki.ru (R.G.C.); Stankevich_VG@nrcki.ru (V.G.S.); FateevVN@nrcki.ru (V.N.F.)
3 DST HySA Infrastructure Centre of Competence, North-West University, Potchefstroom 2520, South Africa; 21220212@nwu.ac.za (S.P.d.P.); dmitri.bessarabov@nwu.ac.za (D.B.)
4 MIREA—Russian Technological University (RTU MIREA), 78, Vernadskiy Ave., Moscow 119454, Russia; evdokimov@mirea.ru
* Correspondence: sergey.grigoriev@outlook.com

Received: 2 March 2019; Accepted: 12 March 2019; Published: 16 March 2019

Abstract: Pt/C and Pt/SnO_x/C catalysts were synthesized using the polyol method. Their structure, morphology and chemical composition were studied using a scanning electron microscope equipped with an energy dispersive X-ray spectrometer, transition electron microscope and X-ray photoelectron spectroscope. Electrochemical measurements were based on the results of rotating disk electrode (RDE) experiments applied to ethanol electrooxidation. The quick evaluation of catalyst activity, electrochemical behavior, and an average number of transferred electrons were made using the RDE technique. The usage of SnO_x (through the carbon support modification) in a binary system together with Pt causes a significant increase of the catalyst activity in ethanol oxidation reaction and the utilization of ethanol.

Keywords: ethanol electrooxidation; rotating disk electrode; Tin; Tin oxide; direct ethanol fuel cell

1. Introduction

There is increasing global interest in hydrogen/fuel cell systems for distributed power generation and transport applications. Currently, steam reforming of hydrocarbons or alcohols is used for the large-scale production of hydrogen [1]. The electrolysis of aqueous alcohols, in particular ethanol (EtOH), has been proposed as a promising method for hydrogen production on site since it has lower power consumption than water electrolysis [2,3]. But it does have some limitations due to sluggish alcohol oxidation kinetics [4,5]. A slow and incomplete ethanol oxidation reaction (EOR) in polymer electrolyte membrane (PEM)-based electrochemical systems is a major drawback to the commercialization of both direct ethanol fuel cells (DEFCs) and electrochemical converters [6].

The selectivity of complete EtOH oxidation is not very important in the case of DEFCs (where power density is a more important output), but it is crucial in the case of EtOH conversion. The electrochemical conversion of EtOH in electrochemical cells with a PEM has been suggested to be a very promising approach to hydrogen generation, because the theoretical cell voltage for the electrochemical decomposition of EtOH is lower than the theoretical cell voltage for water electrolysis [2,7]. Furthermore, because hydrogen is the main target product here, the completeness of EtOH oxidation to carbon dioxide is of great importance.

Possible pathways of the EtOH oxidation reaction are shown in Scheme 1 [8].

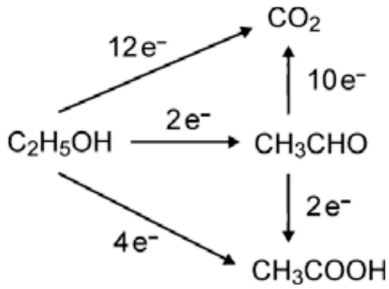

Scheme 1. Possible parallel pathways of EtOH oxidation [8].

The so-called C1 pathway (Equation (1)) proceeds via an adsorbed carbon monoxide (CO_{ads}) intermediate to afford CO_2 by delivering 12 electrons. The so-called C2 pathway (Equations (2) and (3)) mainly leads to the formation of acetic acid by delivering four electrons, and/or acetaldehyde by delivering two electrons [9].

$$CH_3CH_2OH + 3\ H_2O \rightarrow 2\ CO_2 + 12\ H^+ + 12\ e^- \quad (1)$$

$$CH_3CH_2OH \rightarrow CH_3CHO + 2\ e^- + 2\ H^+ \quad (2)$$

$$CH_3CH_2OH + H_2O \rightarrow CH_3CO_2H + 4\ e^- + 4\ H^+ \quad (3)$$

Pure Pt, however, is not an efficient electrocatalyst for EtOH oxidation, being rapidly poisoned by strongly adsorbed species coming from EtOH dissociative adsorption [2]. Currently, bimetallic (alloyed or non-alloyed) PtRu and PtSn are regarded as some of the most efficient catalysts for the EOR because of their bifunctional mechanism [9–13], where dissociative adsorption of EtOH occurs only on Pt sites and Sn (SnO_2) promotes adsorption and dissociation of water to form OH oxidizing intermediates from EtOH [14]. The usage of carbon supports modified with oxophilic oxides particles (RuO_2 or SnO_2) helps to increase the Pt-based catalyst activity and selectivity because these SnO_2 particles protect the Pt active sites from the OH species adsorption at high potentials [15]. In particular, the CO_2 yield using Pt/RuSnOx/C were higher at high potentials than PtRn/C alloyed catalyst [16,17].

Since the efficiency of a DEFC or the electrochemical conversion in a PEM cell is proportional to the average number of electrons transferred per ethanol molecule [14], the reaction stoichiometry is a critical factor in the development of electrochemical applications. Rotating disk electrode (RDE) voltammetry is commonly used to reduce the kinetic current limited by the mass transport [18]. This technique is commonly used as a tool to evaluate the activity of different catalysts in oxygen reduction [19] and hydrogen evolution [20] reactions.

The electrochemical activity of electrocatalysts is usually studied in a three-electrode system under steady-state conditions. However, in real electrochemical applications (fuel cells or electrochemical convertors), the alcohol is supplied to the anode electrode, that is, the system is under hydrodynamic conditions. It is thus important to take into account the effect of fuel transport to the catalyst [21] and the transfer of byproducts through the catalyst layer.

Sayadi and Pickup [22,23] successfully implemented the RDE technique as a useful and practical method for estimating the average number of electrons transferred during the EOR under hydrodynamic conditions and for the evaluation of catalyst activity.

In the present study, Pt/C and Pt/SnO_x/C catalysts with different Sn content were synthesized using the polyol method. Preliminary modification of the Vulcan XC-72 carbon support with SnO_x particles was carried out. Catalysts were evaluated using various methods, including scanning electron microscopy (SEM), energy dispersive X-ray spectrometry (EDS), transition electron microscopy (TEM), X-ray photoelectron spectroscopy (XPS) and RDE voltammetry, using thick catalyst layers. The kinetics

and selectivity in the EOR of the $Pt/SnO_x/C$ catalysts were studied using the Koutecky–Levich approach. Results are discussed in the following sections.

2. Results and Discussion

2.1. Catalyst Characterization

The elemental mapping images and the SEM images (of Pt^{20}/C (A,B), $Pt^{20}/SnO_x{}^{8}/C$ (C–E) and $Pt^{20}/SnO_x{}^{12}/C$ (F–H) catalysts are shown in Figure 1. Pt and Sn are evident and well distributed on the carbon support surface. The catalyst synthesis approach that we applied affords Pt nanoparticles with average sizes of 3.6 nm and with narrow distribution [24] (as confirmed by TEM images below). Data presented in Figure 1 suggest that, generally, Pt and SnO_x particles formed clusters, enabling bifunctional catalysis [25,26] and the porous structure of the catalysts prepared. The Pt distribution becomes less uniform with increasing Sn content, possibly due to the larger size and more agglomerated structure of nanoparticles.

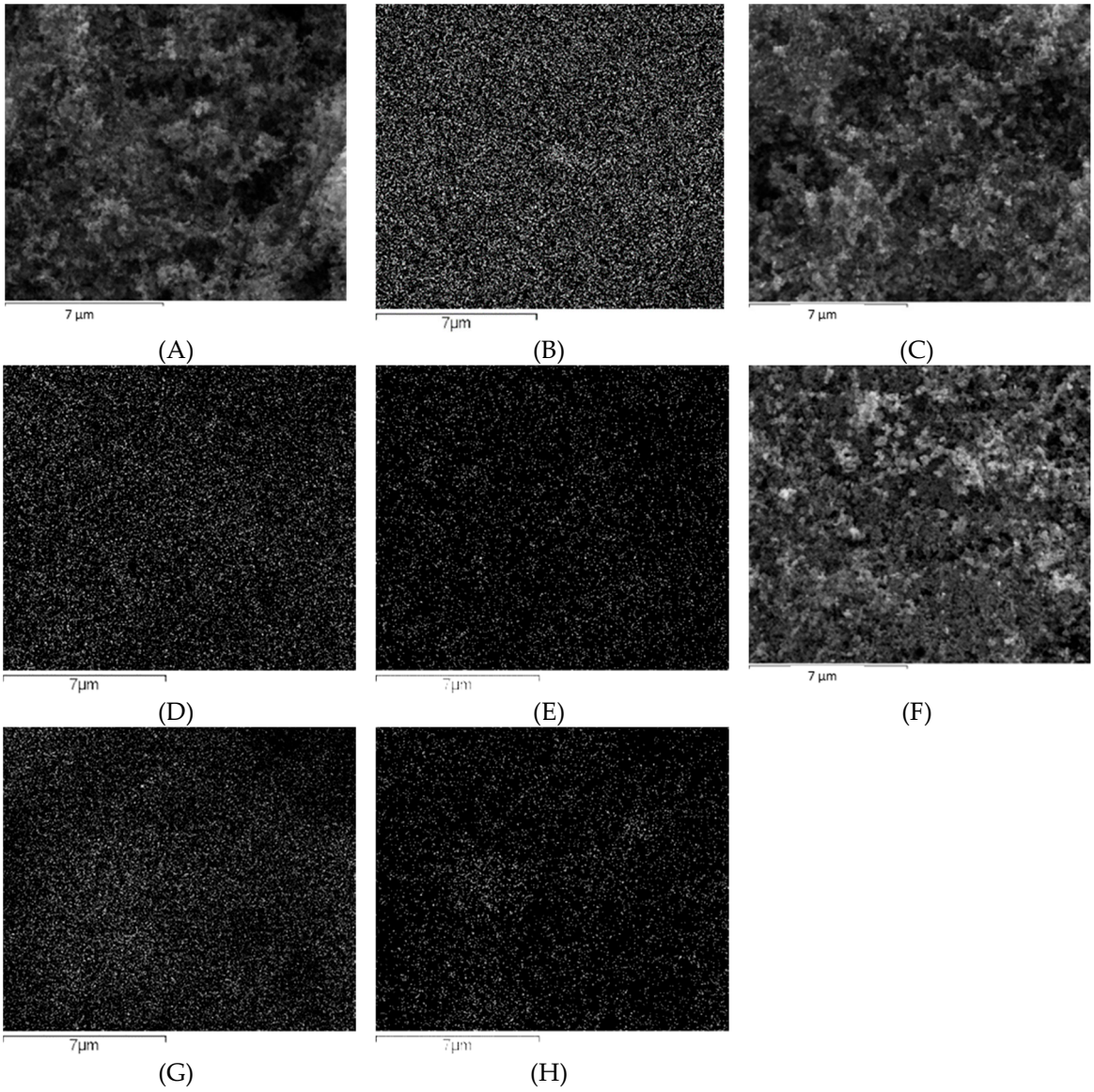

Figure 1. SEM-EDS elemental mapping images of Pt^{20}/C (**A**,**B**), $Pt^{20}/SnO_x{}^{8}/C$ (**C**–**E**) and $Pt^{20}/SnO_x{}^{12}/C$ (**F**–**H**). Pt mapping is shown in (**B**,**D**,**G**); Sn mapping is shown in (**E**,**H**).

The actual Sn content of all catalysts was confirmed by EDS measurements. Data are tabulated in Table 1.

Table 1. EDS elemental content data.

Catalyst	Pt, wt %	Sn, wt %
Pt^{20}/C	19.43	-
$Pt^{20}/SnO_x{}^{8}/C$	20.38	8.37
$Pt^{20}/SnO_x{}^{12}/C$	21.24	11.86

Electrocatalyst morphology and particle size distribution were further characterized by TEM. As can be seen in Figure 2, a uniform dispersion of relatively small particles on the carbon black was accomplished for all synthesized electrocatalyst compositions.

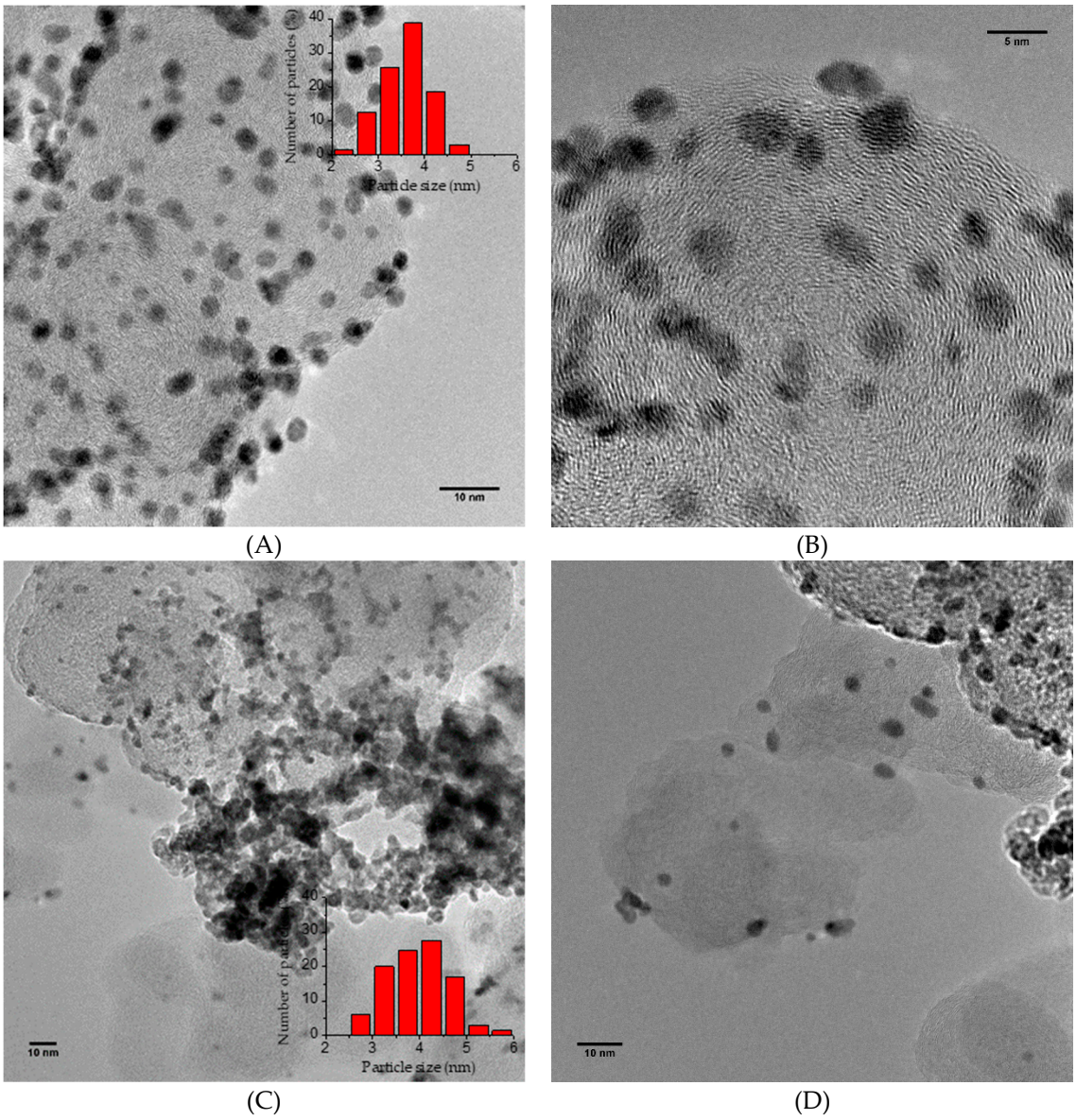

Figure 2. *Cont.*

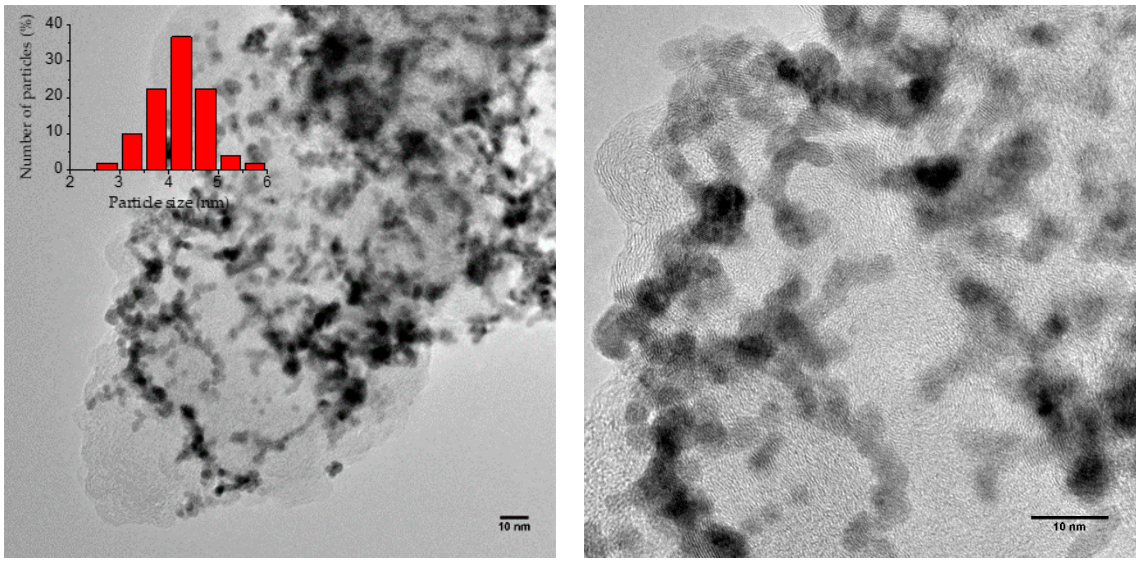

(E) (F)

Figure 2. TEM images of Pt^{20}/C (**A**,**B**), $Pt^{20}/SnO_x{}^{8}/C$ (**C**,**D**) and $Pt^{20}/SnO_x{}^{12}/C$ (**E**,**F**).

The associated histograms in Figure 2, suggesting the round shape of nanoparticles, reveal a narrow particle size distribution with a very similar mean particle size. More than 95% of all Pt/C particles are between 2.5 and 4.5 nm, and for $Pt^{20}/SnO_x{}^{8}/C$ and $Pt^{20}/SnO_x{}^{12}/C$ the size of ca. 90% of all particles are between 3 and 5 nm. The mean particle size of Pt^{20}/C, $Pt^{20}/SnO_x{}^{8}/C$ and $Pt^{20}/SnO_x{}^{12}/C$ is ca. 3.6, 4 and 4.2 nm, respectively. Calculations are based on the size of over 100 Pt particles in TEM images, such as those in Figure 2. However, the structure of $Pt^{20}/SnO_x{}^{8}/C$ and $Pt^{20}/SnO_x{}^{12}/C$ catalysts seem to be strongly agglomerated in comparison with that of Pt^{20}/C. This could be described by the reduced number of active sites for Pt nanoparticles nucleation and further particle merging, or by the Pt selective deposition onto or near the metal oxide phase in the composite support [27,28].

The XPS spectra of Pt and Sn atoms in the corresponding catalysts are presented in Figure 3. For all catalysts, spectra exhibited intense doublets at particular same binding energy of ca. 71.2 and ca. 74.5 that are assigned to $Pt(4f_{7/2})$ and $Pt(4f_{5/2})$ suggesting zero-valent state of Pt [29]. The Sn $3d_{5/2}$ spectrum can be deconvoluted into two peaks attributed to Sn(0) at 485.4 eV and Sn(IV) at 487.1 eV [30–32]. It can be observed that Sn is mostly in its oxidized state for both $Pt^{20}/SnO_x{}^{8}/C$ and $Pt^{20}/SnO_x{}^{12}/C$ catalysts (89–93%). It must be mentioned that these results are applicable to the catalyst surface. The bulk content of SnO_2 could be lower, because metallic Sn has a strong tendency to be re-oxidized after being exposed to air.

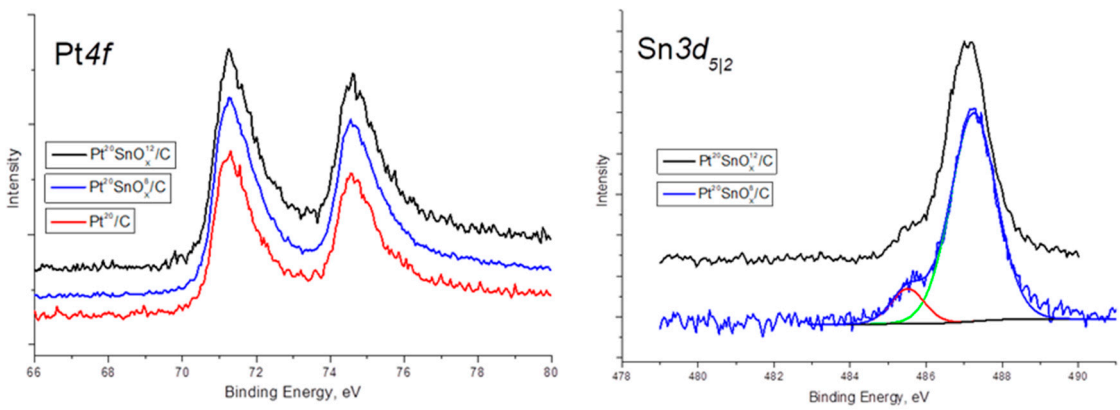

Figure 3. Both Sn $3d_{5/2}$ and Pt 4f XPS profiles of the Pt^{20}/C (only Pt 4f), $Pt^{20}/SnO_x{}^{8}/C$ and $Pt^{20}/SnO_x{}^{12}/C$.

2.2. Electrochemical Measurements

According to cyclic voltammograms (CVs) (Figure 4), all catalysts show well-defined hydrogen adsorption/desorption peaks in the potential region 0.05–0.40 V (vs. SHE—standard hydrogen electrode), and the oxygen adsorption/desorption peaks at about 0.8 and 1.0 V (vs. SHE), specific for Pt-based catalysts [19]. However, a hydrogen adsorption and desorption potential region was inhibited by the presence of Sn in the electrocatalyst. A suppression of currents in this region can be explained by the blockage of Pt adsorption sites [33]. The shape of the CVs is characterized by an increased current in the double layer region between 0.4 and 0.8 V, providing evidence of the existence of Sn species [34]. This could be ascribed to the activation of water on the Sn and SnO_2 species [12,35]. The small peaks that appear around 0.55 and 0.70 V may be attributed to the adsorption/desorption of oxygen-containing species, coming from the dissociation of water on the Sn oxide [26,35,36].

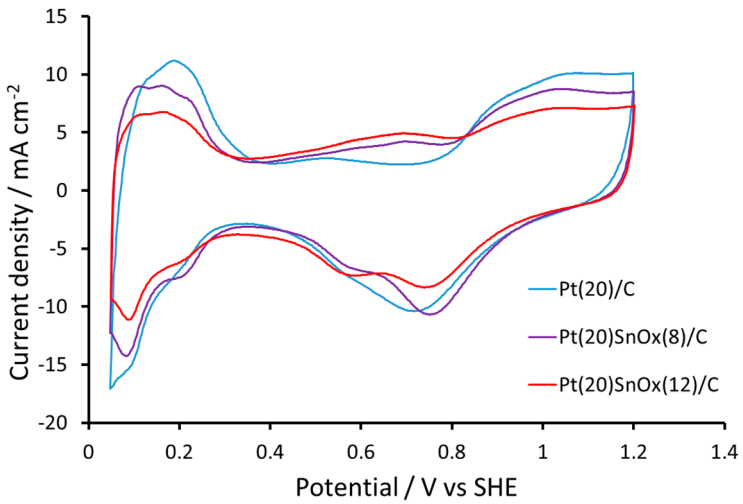

Figure 4. Cyclic voltammograms of electrodes with different catalysts in the supporting electrolyte obtained in an Ar saturated 0.5 M H_2SO_4 solution at 20 mV/s. Currents are normalized to electrode geometric surface area.

The electrochemical active surface area (EASA) of the catalysts was measured. A summary of results is tabulated in Table 2. It should be noted here that the catalyst loading on the working electrode (and hence the catalyst layer thickness) could significantly influence the EASA values [37]. In our work, thick catalyst layers were used; thus, the EASA values could be underestimated (compared with literature data). At the higher SnO_x content, the active surface area is significantly decreased. This could be due to the decrease in carbon black content and because the SnO_x species are able to fill the sites suitable for Pt particle nucleation and thus deteriorate the Pt nanoparticle distribution over the support surface.

Table 2. Catalyst activity parameters.

Catalyst	EASA/m^2 gPt^{-1}	Tafel Slope [1]/mV dec.$^{-1}$	Kinetic Current at 0.8 V/mA cm$^{-2}_{GEOM}$	Kinetic Current at 0.8 V/mA m$^{-2}_{EASA}$
Pt^{20}/C	58.1	619.2	24.2	0.082
$Pt^{20}/SnO_x^{8}/C$	46.1	585.6	29.5	0.126
$Pt^{20}/SnO_x^{12}/C$	26.0	568.4	36.7	0.277

[1] At high voltages (0.6–0.9 V vs. SHE).

According to Figure 5, all samples demonstrate three current waves at ~0.8–1.0 V, and at potentials > 1.1 V on the forward scan and ~0.4–0.8 V on the reverse scan [38]. The regions of inhibition of electrooxidation of organic compounds mainly coincide with the oxygen adsorption regions (>0.8 V).

Actually, the maximum surface oxide coverage of the Pt electrode is achieved at ca. 1.05 V, suppressing the first oxidation wave [39]. In the reverse potential scan, the adsorbed oxide layer is stripped. The second wave during the positive scan may coincide with the dominated acetic acid [40,41] formation and to the formation of more electroactive surface oxides [42]. $Pt^{20}/SnO_x/C$ catalysts demonstrated higher activity than Pt/C due to the higher currents at potentials > 0.8 V. The hydrogen adsorption/desorption regions are less pronounced in the case of Pt/C due to the stronger poisoning of Pt active sites in EtOH solution. Figure 5 shows that the catalyst activity in the EOR increases with increasing Sn content. A further increase in the Sn content leads to a significant decrease in the carbon content, poorer Pt nanoparticle distribution, and extremely low EASA of catalyst, which manifested in lower activity.

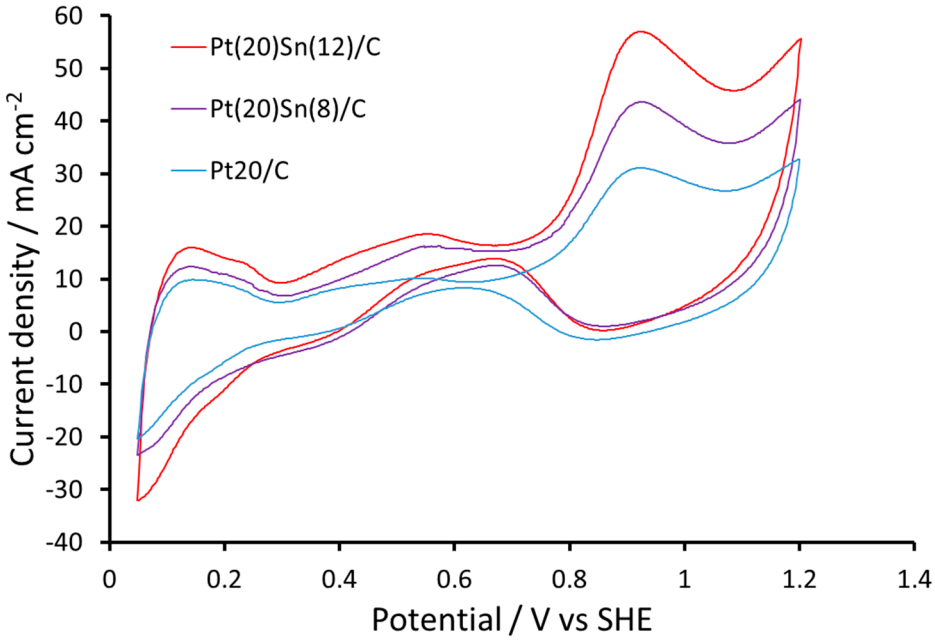

Figure 5. Cyclic voltammograms of EtOH oxidation on electrodes with different catalysts obtained in 0.1 M EtOH solutions (Ar purged) with 0.5 M H_2SO_4 as the supporting electrolyte at 50 mV/s sweep rate. Currents are normalized to electrode geometric surface area.

As it is difficult to achieve the mass transport limited plateau due to the formation of an oxide layer on the Pt surface starting at ca. 0.7–0.8 V, which hinders further EtOH adsorption [22], measurements at constant potentials (0.6–0.9 V vs. SHE) were performed at different electrode rotation speeds. The Koutecky–Levich equation (Equation (4)) was used to estimate the kinetic and mass transport components of the currents measured. For example, the results of potentiostatic measurements at different Pt/C electrode rotation speed at 0.7 V, and the respective Koutecky–Levich plots obtained from this experiment are shown on Figure 6.

$$\frac{1}{i} = \frac{1}{i_k} + \frac{1}{(0.62 \cdot n_{av} \cdot F \cdot A \cdot D^{\frac{2}{3}} \cdot v^{-\frac{1}{6}} \cdot C \cdot \omega^{\frac{1}{2}})} \quad (4)$$

where i (mA) is the measured current, i_k (mA) is the kinetic current, n_{av} is the average number of electrons transferred per EtOH molecule, F (C mole^{-1}) is the Faraday constant, A (cm^2) is the electrode surface area, D (cm^2 s^{-1}) is the diffusion coefficient (a value of $1.22 \cdot 10^{-5}$cm^2 s^{-1} for aqueous EtOH at 25 °C was taken from literature [22]), v (cm^2 s^{-1}) is the kinematic viscosity (taken equal to $1.0 \cdot 10^{-2}$ cm^2 s^{-1} according to the [22]), C (mole L^{-1}) is the EtOH concentration, and ω (s^{-1}) is the electrode angular velocity.

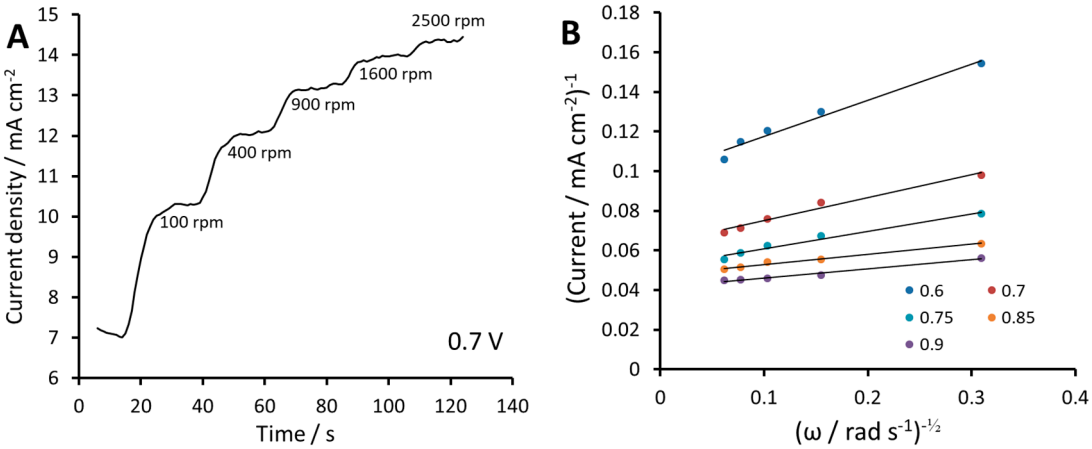

Figure 6. Pt^{20}/C catalyst: (**A**) Experimental constant potential curve measured at different sweep rates (0.7 V vs. SHE) measured in 0.1 M EtOH solutions (Ar purged) with 0.5 M H_2SO_4 as the supporting electrolyte; and (**B**) Koutecky–Levich plots. Currents are normalized to electrode geometric surface area.

At potentials from 0.6 to 0.9 V, all Koutecky–Levich plots showed linear behavior allowing extraction of the transferred electrons number and kinetic current. However, the curves corresponding to the different voltages are not parallel, indicating that n_{av} is potential dependent. At lower potentials (<0.6 V), non-linear behavior of Koutecky–Levich plots was observed. This could be explained by the catalyst surface poisoning by acetaldehyde [22], taking into account that the acetaldehyde is expected to be the major product at low potentials. This suggestion is supported by the n_{av} values (at 0.6 V) increasing for the SnO_x modified catalysts due to the promoted acetaldehyde oxidation on their surface, as discussed below.

The kinetic currents for the catalysts are presented as Tafel plots in Figure 7A,B. The slope of 619 mV decade^{-1} for Pt/C is in good agreement with electrodes that have high mass loading (high catalyst layer thickness) [22]. It is, however, significantly higher than other values reported in literature (132–310 mV) for carbon supported Pt [43–46].

According to Bach Delpeuch et al. [44], the EOR Tafel slope on Pt-Rh-SnO_2/C of ca. 420 mV decade^{-1}, compared with Tafel slopes on Pt/C and Pt-Rh/C, which have values of about 160 mV decade^{-1} and 170–180 mV decade^{-1}, respectively, indicates that the rate-determining step of the EOR differs for Pt-Rh-SnO_2/C and involves the cleavage of the C–C bond. The Tafel slope of the EOR decreased slightly when the SnO_x content increased. The same phenomenon is described by Kuriganova et al. [43]. It should be noted, however, that different Tafel slopes could be obtained depending on the product distribution under specific conditions.

The addition of SnO_2 provided larger kinetic current of EtOH oxidation at 0.6–0.9 V (Figure 7A): up to two-times larger for $Pt^{20}/SnO_x{}^{12}$/C in comparison with Pt^{20}/C. For example, kinetic current values at 0.8 V are presented in Table 2. Kinetic current at 0.8 V for $Pt^{20}/SnO_x{}^{12}$/C is approximately 1.5 times higher in comparison with Pt^{20}/C. Moreover, the effect of SnO_x better pronounced in the kinetic currents normalized to the EASA (i.e., catalyst specific activity). The specific activity of $Pt^{20}/SnO_x{}^{12}$/C at 0.8 V is approximately 3.3 times larger in comparison with Pt^{20}/C (Table 2).

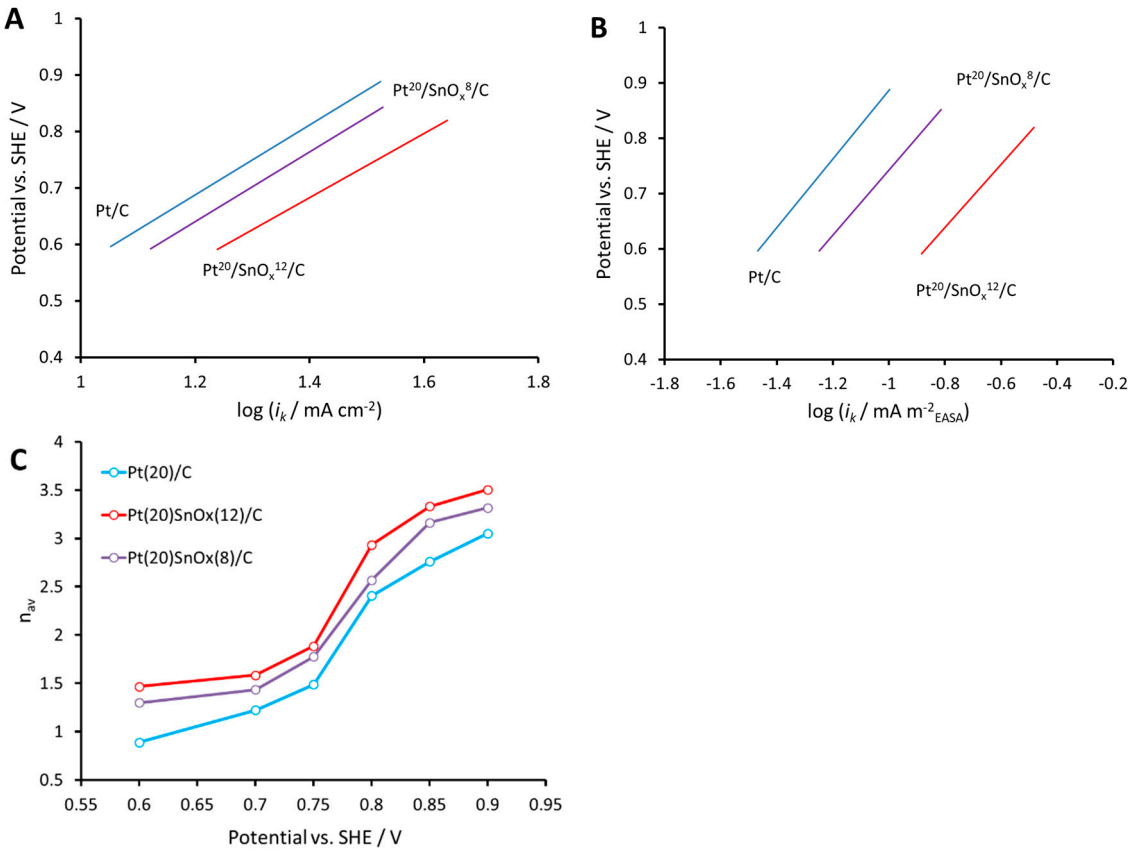

Figure 7. (**A**,**B**) Tafel plots of different catalysts plotted using the kinetic currents obtained from Koutecky–Levich plots, and (**C**) the average number of transferred electrons calculated through Equation (4).

Figure 7C shows an average number of transferred electrons plotted vs. the potential. At low potentials (<0.8 V), we observe an unreasonably low n_{av} (<2) (2 transferred electrons correspond to the complete conversion of EtOH to acetaldehyde (refer to Scheme 1)). This low value could be explained by the enhanced convective diffusion of acetaldehyde away from the disk electrode with an increase in rotation rate, leading to the underestimated n_{av} value [22]. The following increase of n_{av} at higher potentials (>0.8 V) is in a good agreement with results of Sayadi and Pickup [22] for the Pt^{20}/C catalyst.

The SnO_x provided the n_{av} increasing by 0.35–0.60 in the full potential range being studied. This could be related to the higher activity in both CO_2 or acetic acid yield. Similar behavior of the plots in Figure 7B suggests that the same EOR mechanism applies for both the Pt^{20}/C and Pt^{20}/SnO_x/C catalysts. According to literature [6,25,47], SnO_x can provide adsorbed OH (OH_{ads}) species from water dissociation to remove the strongly adsorbed intermediate products at adjacent Pt active sites in accordance with the bifunctional mechanism. OH_{ads} species enhanced the further oxidation of chemisorbed CO_{ads} intermediates (product of C–C bond splitting together with CH_x compounds) to CO_2 [25]. However, the addition of Sn (SnO_2) to Pt tends to promote the partial oxidation of acetaldehyde to acetic acid and does not specifically enhance C–C bond cleavage during the EOR [9,47–49]. DFT calculations [50] have shown that the formation of OH species on the Pt surface leads to a significantly increased reaction barrier for C–C bond cleavage and consequently inhibits CO_{ads} formation and CO_2 production. At high potentials (0.8–0.9 V) the n_{av} is close to four, which could correspond to the near-complete EtOH oxidation to acetic acid (refer to Scheme 1). However, the apparent n_{av} value could not be used as a measure of any catalyst selectivity towards CO_2 or

other products. Even according to the simplified EtOH oxidation pathways (Scheme 1), we should determine the n_{av} according to Equation (5):

$$n_{av} = \sum n_i f_i, \tag{5}$$

where n_{av} is the average number of electrons transferred per EtOH molecule; and n_i is the is the number of electrons transferred to form product i and f_i is the fraction of ethanol converted to product i. The apparent value of n_{av} could come from different combinations of products and their yields (f_i and n_i), depending on mechanism pathways, catalyst surface structure, and experimental conditions [5,9,51–53]. Thus, the entire understanding of reaction mechanism on synthesized catalysts is possible only when using a full product analysis approach. It should be noted that the RDE technique that we used is not sufficiently accurate at potentials < 0.5 V (as mentioned above); hence, it is difficult to discuss the CO_2 catalyst selectivity because the CO_2 is preferably produced on Pt at low potentials [6]. Furthermore, the experimental conditions should be taken into account. Here, for example, the temperature increase up to 90 °C could increase the CO_2 yield [54]. Moreover, according to Camara and Iwasita, CO_2 evolution is more pronounced at low EtOH concentrations (<0.1 M), with negligible acetaldehyde [8]. Recently, an effective PEM-based cell approach was established [55–57], which enables one to accurately determine the n_{av} and stoichiometry of the EOR using the PEM electrolysis cell operated in crossover mode. The thick-film RDE technique that we used, and describe here, could nonetheless be used as an approach for quick catalyst screening.

3. Materials and Methods

3.1. Pt/SnO$_x$/C Catalyst Synthesis

The following procedure was followed to prepare the Pt/SnO$_x$/C catalysts. First, the carbon support Vulcan XC-72 (Cabot, Boston, MA, USA) was modified with SnO$_x$. Second, a three-neck flask with ethylene glycol (EG) was charged with a calculated amount of $SnCl_2$*$2H_2O$ dissolved in EG and a small volume of deionized (DI) water. The reaction mixture was refluxed for 3 h at 190 °C under constant magnetic stirring until the color of the solution changed to slightly yellow. The obtained colloidal SnO$_x$ particles were cooled to room temperature (rt). A calculated amount of the support (Vulcan XC-72), DI water, and isopropyl alcohol were mixed together and then added dropwise to the preheated (to 50 °C) colloidal SnO$_x$ particles under magnetic stirring. Adsorption of the SnO$_x$ particles onto the support surface was carried out over a period of for 48 h at rt, under constant magnetic stirring.

Preparation of the Pt electrocatalyst on a carbon support was carried out using the polyol synthesis procedure. An aqueous solution of H_2PtCl_6*$2H_2O$ was used as Pt particles precursor. The solution was added dropwise to an EG solution of the carbon support, under magnetic stirring. The reaction was carried out at rt for 30 min under an Ar atmosphere. The temperature was then gradually increased (at a rate of 1 °C min^{-1}) to 75 °C and the precursor adsorption was carried out over 2 h. Thereafter, the temperature was rapidly increased to 180 °C and the Pt reduction was carried out for 1 h. The suspension was then cooled to rt and the pH was decreased to 6, using an HCl solution. Finally, the catalyst powder was filtered and washed with DI water at least three times. The resulting catalyst was dried at 70 °C overnight. The Pt content of all the catalysts was 20 wt. %.

3.2. Electrode Preparation

Thick catalyst films on a polished glassy carbon disk electrode (0.196 cm^2; Pine Instruments, Durham, NC, USA) were prepared by dropping catalyst ink with an Eppendorf micropipette (catalyst loading 3 mg cm^{-2}). The specified catalyst loading is given without the inclusion of Nafion, used as a binder, which was 30 wt. % of the specified catalyst weight

Catalyst inks were prepared by ultrasound treatment. First, a mixture consisting of the weighted amount of catalyst powder in DI water was treated in an ultrasound bath for 1 h. This was followed

by the addition of 10% Nafion solution (Ion Power, Navarre, FL, USA) and further ultrasonication for 10 min (finally, the catalyst amount was ca. 30 mg mL^{-1}). Each catalyst layer was dried at 40 °C.

Rather high catalyst loadings are required to obtain meaningful results due to the possible fast transport of EOR products away from the electrode at low catalyst layer thickness [22]. Thus, in our work described here, a catalyst loading of 3 mg cm^{-2} was used. A higher catalyst loading was unachieved due to the lower mechanical stability of the catalyst layer.

3.3. Electrochemical Measurements

Electrochemical experiments were performed at 25 °C in a three-electrode glass cell (Pine Instruments) equipped with a polished glassy carbon working electrode, a Pt wire counter electrode (Pine Instruments) placed in a fritted glass tube, and Ag/AgCl/sat. KCl reference electrode (Pine Instruments) connected to the electrochemical cell by a Luggin capillary. A SP-150 potentiostat (BioLogic, Seyssinet-Pariset, France) and MSR rotator (Pine Instruments) were used at HySA Infrastructure facilities in South Africa. All potentials are given relative to the SHE. All EtOH oxidation experiments were carried out in 0.1 M EtOH solutions (Ar purged) with 0.5 M H_2SO_4 as the supporting electrolyte.

The electrode was activated in an Ar saturated 0.5 M H_2SO_4 solution at a potential range of 0.05–1.40 V for about 25–30 cycles at a 50 mV/s sweep rate until a stable CV was obtained. CVs at 20 mV/s at potentials ranging from 0.05 to 1.20 V were then recorded to determine the catalyst behavior. These CV curves were also used to determine the EASA of the catalysts from the integrated charge in the H_2 desorption region (0.05–0.40 V vs. RHE, a reversible hydrogen electrode). Pt surface areas were determined by cyclic voltammetry (see Section 2.2) in 0.5 M H_2SO_4 at 20 mV/s sweep rate. The EASA value (m^2 g^{-1}Pt) could be calculated as follows:

$$EASA = \frac{Q_H}{10 \cdot Q_0 \cdot m_{Pt}}, \tag{6}$$

where Q_H (mQ cm^{-2}) represents the H_2 desorption charge, m_{Pt} (mg cm^{-2}) is the Pt loading, and Q_0 is the charge required to oxidize the monolayer of hydrogen on a Pt surface [37].

3.4. Catalysts Structure and Morphology Characterization

A scanning electron microscope equipped with an energy dispersive X-ray spectrometer was used to perform the surface chemical characterization of samples. A FEG Quanta 250 SEM instrument (FEI, Netherlands) incorporating an Oxford X-map EDS system, operating at 15 kV and a working distance of 10 mm, was used. Samples were mounted onto aluminum stubs using adhesive tape prior to SEM-EDS analysis procedures. These samples were left uncoated. Transmission electron microscopy was performed using Titan TM 80-300 S/TEM (FEI, Hillsboro, OR, USA). Samples were prepared by ultrasonic treatment of catalyst in EtOH for 12 min followed by pipetting the mixture onto a Lacey (thin, X-ray amorphous) carbon film supported on a copper grid. The XPS study of catalysts were performed on a PHOIBOS 150 (Berlin, Germany) hemispherical analyzer (Al Kα radiation) with 1486.61 eV photon energy at ΔE = 0.2 eV.

4. Conclusions

The thick-film RDE technique (first proposed by Sayadi and Pickup in 2016 [22]) is suitable for the evaluation of Pt/SnO_x/C supported catalysts activity in the EOR and for evaluating the reaction selectivity in the high potential region. This is a hydrodynamic method which mimics the DEFC and electrochemical EtOH converter anode working conditions (including high thickness of the catalytic layer), and it could be used for quick EOR catalyst activity evaluation. According to our results, the SnO_x addition could increase the efficiency of EtOH consumption in a DEFC or EtOH electrochemical converter through a high yield of acetic acid providing a significantly higher (3.3 times

higher current at 0.8 V in comparison with Pt/C) kinetic current and increased average number of electrons (by 0.35–0.60) transferred in full potential range being studied. Considerable activity growth was achieved despite the certain Pt EASA reduction with increasing SnO_x content. Large CO_2 selectivity of a Pt-based catalyst could be achieved through the rational design of catalyst that takes into account not only the usage of the OH_{ads}, providing component (SnO_x), but also a suitable catalyst surface composition, and suitable surface sites for C–C bond cleavage (which could be provided, for example, by using the Rh as the third catalyst component).

Author Contributions: Conceptualization, A.S.P. and D.B.; methodology, A.S.P. and D.B.; software, S.P.d.P.; validation, I.V.P. and N.A.I.; formal analysis, A.S.P., A.A.E.; investigation, A.S.P., I.V.P., R.G.C. and V.G.S.; resources, D.B. and V.N.F.; data curation, N.A.I.; writing—original draft preparation, A.S.P. and I.V.P.; writing—review and editing, S.A.G. and D.B.; visualization, S.P.d.P.; supervision, S.A.G.; project administration, S.A.G.; funding acquisition, S.A.G.

Funding: The synthesis of catalysts, and their electrochemical and morphological studies, were financially supported by the Russian Foundation for Basic Research (project no. 16-08-01070 a). The modification of carbon support with SnO_x was executed within the framework of government assignment of the Ministry of Science and Higher Education of the Russian Federation (project no. 13.2052.2017/4b). Studies performed in NRC "Kurchatov institute" was supported by project no. 1390.

Conflicts of Interest: The authors declare no conflict of interest.

References

1. Holladay, J.D.; Hu, J.; King, D.L.; Wang, Y. An overview of hydrogen production technologies. *Catal. Today* **2009**, *139*, 244–260. [CrossRef]
2. Lamy, C.; Jaubert, T.; Baranton, S.; Coutanceau, C. Clean hydrogen generation through the electrocatalytic oxidation of ethanol in a Proton Exchange Membrane Electrolysis Cell (PEMEC): Effect of the nature and structure of the catalytic anode. *J. Power Sources* **2014**, *245*, 927–936. [CrossRef]
3. Caravaca, A.; Sapountzi, F.M.M.; de Lucas-Consuegra, A.; Molina-Mora, C.; Dorado, F.; Valverde, J.L.L. Electrochemical reforming of ethanol–water solutions for pure H2 production in a PEM electrolysis cell. *Int. J. Hydrogen Energy* **2012**, *37*, 9504–9513. [CrossRef]
4. Ju, H.K.; Giddey, S.; Badwal, S.P.S.; Mulder, R.J. Electro-catalytic conversion of ethanol in solid electrolyte cells for distributed hydrogen generation. *Electrochim. Acta* **2016**, *212*, 744–757. [CrossRef]
5. Wang, H.; Jusys, Z.; Behm, R.J. Ethanol Electrooxidation on a Carbon-Supported Pt Catalyst: Reaction Kinetics and Product Yields. *J. Phys. Chem. B* **2004**, *108*, 19413–19424. [CrossRef]
6. Li, M.; Cullen, D.A.; Sasaki, K.; Marinkovic, N.S.; More, K.; Adzic, R.R. Ternary electrocatalysts for oxidizing ethanol to carbon dioxide: Making Ir capable of splitting C-C bond. *J. Am. Chem. Soc.* **2013**, *135*, 132–141. [CrossRef]
7. Pushkareva, I.V.; Pushkarev, A.S.; Grigoriev, S.A.; Lyutikova, E.K.; Akel'kina, S.V.; Osina, M.A.; Slavcheva, E.P.; Fateev, V.N. Electrochemical conversion of aqueous ethanol solution in an electrolyzer with a solid polymer electrolyte. *Russ. J. Appl. Chem.* **2016**, *89*, 2109–2111. [CrossRef]
8. Camara, G.A.; Iwasita, T. Parallel pathways of ethanol oxidation: The effect of ethanol concentration. *J. Electroanal. Chem.* **2005**, *578*, 315–321. [CrossRef]
9. Wang, Y.; Zou, S.; Cai, W.-B. Recent Advances on Electro-Oxidation of Ethanol on Pt- and Pd-Based Catalysts: From Reaction Mechanisms to Catalytic Materials. *Catalysts* **2015**, *5*, 1507–1534. [CrossRef]
10. Antolini, E.; Gonzalez, E.R. Effect of synthesis method and structural characteristics of Pt–Sn fuel cell catalysts on the electro-oxidation of CH3OH and CH3CH2OH in acid medium. *Catal. Today* **2011**, *160*, 28–38. [CrossRef]
11. Ermete, A. Catalysts for direct ethanol fuel cells. *J. Power Sources* **2007**, *170*, 1–12. [CrossRef]
12. Li, H.; Sun, G.; Cao, L.; Jiang, L.; Xin, Q. Comparison of different promotion effect of PtRu/C and PtSn/C electrocatalysts for ethanol electro-oxidation. *Electrochim. Acta* **2007**, *52*, 6622–6629. [CrossRef]
13. Kamarudin, M.Z.F.; Kamarudin, S.K.; Masdar, M.S.; Daud, W.R.W. Review: Direct ethanol fuel cells. *Int. J. Hydrogen Energy* **2013**, *38*, 9438–9453. [CrossRef]

14. Vigier, F.; Coutanceau, C.; Perrard, A.; Belgsir, E.M.; Lamy, C. Development of anode catalysts for a direct ethanol fuel cell. *J. Appl. Electrochem.* **2004**, *34*, 439–446. [CrossRef]
15. Yang, G.; Namin, L.M.; Aaron Deskins, N.; Teng, X. Influence of ∗OH adsorbates on the potentiodynamics of the CO_2 generation during the electro-oxidation of ethanol. *J. Catal.* **2017**, *353*, 335–348. [CrossRef]
16. James, D.D.; Moghaddam, R.B.; Chen, B.; Pickup, P.G. Ruthenium-Tin Oxide/Carbon Supported Platinum Catalysts for Electrochemical Oxidation of Ethanol in Direct Ethanol Fuel Cells. *J. Electrochem. Soc.* **2018**, *165*, F215–F219. [CrossRef]
17. Chen, B.; Brueckner, T.M.; Altarawneh, R.M.; Pickup, P.G. Composition Dependence of Ethanol Oxidation at Ruthenium-Tin Oxide/Carbon Supported Platinum Catalysts. *J. Electrochem. Soc.* **2018**, *165*, J3019–J3025. [CrossRef]
18. Schmidt, T.J.; Gasteiger, H.A. Rotating thin-film method for supported catalysts. In *Handbook of Fuel Cells*; John Wiley & Sons: Chichester, UK, 2003; pp. 316–333, ISBN 9780470974001.
19. Gasteiger, H.A.; Kocha, S.S.; Sompalli, B.; Wagner, F.T. Activity benchmarks and requirements for Pt, Pt-alloy, and non-Pt oxygen reduction catalysts for PEMFCs. *Appl. Catal. B Environ.* **2005**, *56*, 9–35. [CrossRef]
20. Schmidt, T.J. Characterization of High-Surface-Area Electrocatalysts Using a Rotating Disk Electrode Configuration. *J. Electrochem. Soc.* **1998**, *145*, 2354. [CrossRef]
21. Puthiyapura, V.K.; Lin, W.F.; Russell, A.E.; Brett, D.J.L.; Hardacre, C. Effect of Mass Transport on the Electrochemical Oxidation of Alcohols Over Electrodeposited Film and Carbon-Supported Pt Electrodes. *Top. Catal.* **2018**, *61*, 240–253. [CrossRef]
22. Sayadi, A.; Pickup, P.G. Evaluation of ethanol oxidation catalysts by rotating disc voltammetry. *Electrochim. Acta* **2016**, *215*, 84–92. [CrossRef]
23. Sayadi, A.; Pickup, P.G. Evaluation of methanol oxidation catalysts by rotating disc voltammetry. *Electrochim. Acta* **2016**, *199*, 12–17. [CrossRef]
24. Grigoriev, S.A.; Fateev, V.N.; Pushkarev, A.S.; Pushkareva, I.V.; Ivanova, N.A.; Kalinichenko, V.N.; Presnyakov, M.Y.; Wei, X. Reduced Graphene Oxide and Its Modifications as Catalyst Supports and Catalyst Layer Modifiers for PEMFC. *Materials (Basel)* **2018**, *11*, 1405. [CrossRef] [PubMed]
25. Magee, J.W.; Zhou, W.P.; White, M.G. Promotion of Pt surfaces for ethanol electro-oxidation by the addition of small SnO2 nanoparticles: Activity and mechanism. *Appl. Catal. B Environ.* **2014**, *152–153*, 397–402. [CrossRef]
26. Lim, D.-H.; Choi, D.-H.; Lee, W.-D.; Park, D.-R.; Lee, H.-I. The Effect of Sn Addition on a Pt/C Electrocatalyst Synthesized by Borohydride Reduction and Hydrothermal Treatment for a Low-Temperature Fuel Cell. *Electrochem. Solid State Lett.* **2007**, *10*, B87. [CrossRef]
27. Ruiz-Camacho, B.; Santoyo, H.H.R.H.H.R.; Medina-Flores, J.M.J.M.; Álvarez-Martínez, O.; Martínez-Álvarez, O. Platinum deposited on TiO2-C and SnO2-C composites for methanol oxidation and oxygen reduction. *Electrochim. Acta* **2014**, *120*, 344–349. [CrossRef]
28. Kou, R.; Shao, Y.; Mei, D.; Nie, Z.; Wang, D.; Wang, C.; Viswanathan, V.V.; Park, S.; Aksay, I.A.; Lin, Y.; et al. Stabilization of Electrocatalytic Metal Nanoparticles at Metal−Metal Oxide−Graphene Triple Junction Points. *J. Am. Chem. Soc.* **2011**, *133*, 2541–2547. [CrossRef] [PubMed]
29. Lei, F.; Li, Z.; Ye, L.; Wang, Y.; Lin, S. One-pot synthesis of Pt/SnO_2/GNs and its electro-photo-synergistic catalysis for methanol oxidation. *Int. J. Hydrogen Energy* **2016**, *41*, 255–264. [CrossRef]
30. Zhu, M.; Sun, G.; Xin, Q. Effect of alloying degree in PtSn catalyst on the catalytic behavior for ethanol electro-oxidation. *Electrochim. Acta* **2009**, *54*, 1511–1518. [CrossRef]
31. Li, X.-L.; Lin, B.-Z.; Xu, B.-H.; Chen, Z.-J.; Wang, Q.-Q.; Kuang, J.-D.; Zhu, H. Preparation and characterization of mesoporous SnO2-pillared HTaWO6 with enhanced photocatalytic activity. *J. Mater. Chem.* **2010**, *20*, 3924. [CrossRef]
32. Taylor, J.A.; Merchant, S.M.; Perry, D.L. Study of the oxidation of gold-tin preforms using x-ray photoelectron spectroscopy. *J. Appl. Phys.* **1995**, *78*, 5356–5361. [CrossRef]
33. Rizo, R.; Sebastián, D.; Lázaro, M.J.; Pastor, E. On the design of Pt-Sn efficient catalyst for carbon monoxide and ethanol oxidation in acid and alkaline media. *Appl. Catal. B Environ.* **2017**, *200*, 246–254. [CrossRef]

34. Silva, J.C.M.; De Souza, R.F.B.; Parreira, L.S.; Neto, E.T.; Calegaro, M.L.; Santos, M.C. Ethanol oxidation reactions using SnO_2@Pt/C as an electrocatalyst. *Appl. Catal. B Environ.* **2010**, *99*, 265–271. [CrossRef]
35. Lim, D.H.; Choi, D.H.; Lee, W.D.; Lee, H.I. A new synthesis of a highly dispersed and CO tolerant PtSn/C electrocatalyst for low-temperature fuel cell; its electrocatalytic activity and long-term durability. *Appl. Catal. B Environ.* **2009**, *89*, 484–493. [CrossRef]
36. Arenz, M.; Stamenkovic, V.; Blizanac, B.B.; Mayrhofer, K.J.; Markovic, N.M.; Ross, P.N. Carbon-supported Pt-Sn electrocatalysts for the anodic oxidation of H_2, CO, and H_2/CO mixtures.: Part II: The structure-activity relationship. *J. Catal.* **2005**, *232*, 402–410. [CrossRef]
37. Pozio, A.; de Francesco, M.; Cemmi, A.; Cardellini, F.; Giorgi, L. Comparison of high surface Pt/C catalysts by cyclic voltammetry. *J. Power Sources* **2002**, *105*, 13–19. [CrossRef]
38. Tarasevich, M.R.; Korchagin, O.V.; Kuzov, A. V Electrocatalysis of anodic oxidation of ethanol. *Russ. Chem. Rev.* **2013**, *82*, 1047–1065. [CrossRef]
39. Angerstein-Kozlowska, H.; Conway, B.E.; Sharp, W.B.A. The real condition of electrochemically oxidized platinum surfaces. *J. Electroanal. Chem. Interfacial Electrochem.* **1973**, *43*, 9–36. [CrossRef]
40. Leung, L.W.H.; Weaver, M.J. Real-time FTIR spectroscopy as a quantitative kinetic probe of competing electrooxidation pathways of small organic molecules. *J. Phys. Chem.* **1988**, *92*, 4019–4022. [CrossRef]
41. Fujiwara, N.; Friedrich, K.A.; Stimming, U. Ethanol oxidation on PtRu electrodes studied by differential electrochemical mass spectrometry. *J. Electroanal. Chem.* **1999**, *472*, 120–125. [CrossRef]
42. Seland, F.; Foss, C.E.L.; Tunold, R.; Harrington, D. Increasing and Decreasing Mass Transport Effects in the Oxidation of Small Organic Molecules. *ECS Trans.* **2010**, *28*, 203–210. [CrossRef]
43. Kuriganova, A.B.; Leontyeva, D.V.; Ivanov, S.; Bund, A.; Smirnova, N.V. Electrochemical dispersion technique for preparation of hybrid MOx–C supports and Pt/MOx–C electrocatalysts for low-temperature fuel cells. *J. Appl. Electrochem.* **2016**, *46*, 1245–1260. [CrossRef]
44. Bach Delpeuch, A.; Asset, T.; Chatenet, M.; Cremers, C. Influence of the temperature for the ethanol oxidation reaction (EOR) on Pt/C, Pt-Rh/C and Pt-Rh-SnO_2/C. *Fuel Cells* **2015**, *15*, 352–360. [CrossRef]
45. Katikawong, P.; Ratana, T.; Veerasai, W. Temperature dependence studies on the electro-oxidation of aliphatic alcohols with modified platinum electrodes. *J. Chem. Sci.* **2009**, *121*, 329–337. [CrossRef]
46. Baranova, E.A.A.; Tavasoli, A.; Amir, T. Particle Size Effect of Unsupported Pt/SnOx Nanoparticles for Ethanol Electro-Oxidation. *Electrocatalysis* **2011**, *2*, 89–95. [CrossRef]
47. Jiang, L.; Colmenares, L.; Jusys, Z.; Sun, G.Q.; Behm, R.J. Ethanol electrooxidation on novel carbon supported Pt/SnOx/C catalysts with varied Pt:Sn ratio. *Electrochim. Acta* **2007**, *53*, 377–389. [CrossRef]
48. Wang, Q.; Sun, G.Q.; Jiang, L.H.; Xin, Q.; Sun, S.G.; Jiang, Y.X.; Chen, S.P.; Jusys, Z.; Behm, R.J. Adsorption and oxidation of ethanol on colloid-based Pt/C, PtRu/C and Pt3Sn/C catalysts: In situ FTIR spectroscopy and on-line DEMS studies. *Phys. Chem. Chem. Phys.* **2007**, *9*, 2686–2696. [CrossRef] [PubMed]
49. Bach Delpeuch, A.; Maillard, F.; Chatenet, M.; Soudant, P.; Cremers, C. Ethanol oxidation reaction (EOR) investigation on Pt/C, Rh/C, and Pt-based bi- and tri-metallic electrocatalysts: A DEMS and in situ FTIR study. *Appl. Catal. B Environ.* **2016**, *181*, 672–680. [CrossRef]
50. Kavanagh, R.; Cao, X.M.; Lin, W.F.; Hardacre, C.; Hu, P. Origin of low CO_2 selectivity on platinum in the direct ethanol fuel cell. *Angew. Chemie Int. Ed.* **2012**, *51*, 1572–1575. [CrossRef]
51. Rousseau, S.; Coutanceau, C.; Lamy, C.; Léger, J.-M. Direct ethanol fuel cell (DEFC): Electrical performances and reaction products distribution under operating conditions with different platinum-based anodes. *J. Power Sources* **2006**, *158*, 18–24. [CrossRef]
52. Wang, H.-F.; Liu, Z.-P. Comprehensive Mechanism and Structure-Sensitivity of Ethanol Oxidation on Platinum: New Transition-State Searching Method for Resolving the Complex Reaction Network. *J. Am. Chem. Soc.* **2008**, *130*, 10996–11004. [CrossRef] [PubMed]
53. Asiri, H.A.; Anderson, A.B. Mechanisms for Ethanol Electrooxidation on Pt(111) and Adsorption Bond Strengths Defining an Ideal Catalyst. *J. Electrochem. Soc.* **2015**, *162*, F115–F122. [CrossRef]
54. Rao, V.; Cremers, C.; Stimming, U.; Cao, L.; Sun, S.; Yan, S.; Sun, G.; Xin, Q. Electro-oxidation of Ethanol at Gas Diffusion Electrodes A DEMS Study. *J. Electrochem. Soc.* **2007**, *154*, B1138. [CrossRef]
55. Altarawneh, R.M.; Majidi, P.; Pickup, P.G. Determination of the efficiency of ethanol oxidation in a proton exchange membrane electrolysis cell. *J. Power Sources* **2017**, *351*, 106–114. [CrossRef]

56. Altarawneh, R.M.; Pickup, P.G. Determination of the Stoichiometry of Ethanol Oxidation from the Flow Rate Dependence of the Current in a Proton Exchange Membrane Electrolysis Cell. *J. Electrochem. Soc.* **2018**, *165*, F479–F483. [CrossRef]
57. Altarawneh, R.M.; Brueckner, T.M.; Chen, B.; Pickup, P.G. Product distributions and efficiencies for ethanol oxidation at PtNi octahedra. *J. Power Sources* **2018**, *400*, 369–376. [CrossRef]

© 2019 by the authors. Licensee MDPI, Basel, Switzerland. This article is an open access article distributed under the terms and conditions of the Creative Commons Attribution (CC BY) license (http://creativecommons.org/licenses/by/4.0/).